IEIE Transactions on Smart Processing and Computing, vol. 3, no. 2, April 2014
http://dx.doi.org/10.5573/IEIESPC.2014.3.2.41

Minimum Statistics-Based Noise Power Estimation for Parametric Image Restoration

Yoonjong Yoo[1], Jeongho Shin[2], and Joonki Paik[3]

[1] Image Processing and Intelligent Systems Laboratory, Department of Advanced Imaging, Graduate School of Advanced Imaging Science, Multimedia, and Film, Chung-Ang University / Seoul, Korea whitener@cau.ac.kr
[2] Department of Web information Engineering Hankyong University / Gyeonggi, Korea shinj@hknu.ac.kr
[3] Image Processing and Intelligent Systems Laboratory, Department of Advanced Imaging, Graduate School of Advanced Imaging Science, Multimedia, and Film, Chung-Ang University / Seoul, Korea paikj@cau.ac.kr

***** Corresponding Author: Joonki Paik

Received November 20, 2013; Revised December 27, 2013; Accepted February 12, 2014; Published April 30, 2014

** Regular Paper*

***Abstract*:** This paper describes a method to estimate the noise power using the minimum statistics approach, which was originally proposed for audio processing. The proposed minimum statistics-based method separates a noisy image into multiple frequency bands using the three-level discrete wavelet transform. By assuming that the output of the high-pass filter contains both signal detail and noise, the proposed algorithm extracts the region of pure noise from the high frequency band using an appropriate threshold. The region of pure noise, which is free from the signal detail part and the DC component, is well suited for minimum statistics condition, where the noise power can be extracted easily. The proposed algorithm reduces the computational load significantly through the use of a simple processing architecture without iteration with an estimation accuracy greater than 90% for strong noise at 0 to 40dB SNR of the input image. Furthermore, the well restored image can be obtained using the estimated noise power information in parametric image restoration algorithms, such as the classical parametric Wiener or ForWaRD image restoration filters. The experimental results show that the proposed algorithm can estimate the noise power accurately, and is particularly suitable for fast, low-cost image restoration or enhancement applications.

***Keywords*:** Power Estimation, Noise Estimation, Restoration

1. Introduction

Image restoration estimates the original undistorted image from an observed image using an inverse operation of various image degradation factors, such as out-of-focus, motion blur, and atmospheric turbulence, in an imaging system. In particular, based on the image degradation model, the image restoration process is considered adeconvolution of the point spread function (PSF) or statistical inverse problem (SIP). Because image restoration is almost always an ill-posed problem, its solution either does not exist or it is not unique. This results in a set of feasible solutions rather than a unique one. *A priori* information of the original image is used most widely to select the best solution in the set. This type of image restoration approach includes a Wiener filter, constrained least squares (CLS) filter, and iterative regularization, all of which fall into the category of regularized image restoration [1].

A parametric Wiener filter approximates the noise-to-signal power ratio (NSPR) to a constant for simplified, efficient realization. On the other hand, the CLS filter and iterative regularization incorporate *a priori* information as a form of a regularization constraint into the solution. The relative amount of the regularization constraint is controlled by a regularization parameter. The abovementioned image restoration methods are called parametric image restoration because they use a single parameter to control the amount of regularization. Among the various sophisticated image restoration approaches available, a parametric image restoration is particularly suitable for efficient, realistic applications, such as digital auto-focusing and motion blur removal using an embedded processor or a system on chip (SOC). For the successful

deployment of parametric image restoration to the real imaging system, an accurate estimation of noise power is of paramount importance because the regularization parameter is related directly to the noise power.

Although many image denoising methods for image enhancement have been proposed, their application to parametric image restoration exhibits limited performance because they mainly extract the original signal instead of estimating the noise power [2, 3]. On the other hand, blind deconvolution is considered to be the most fundamental approach to estimating the original image without information on the image degradation model and noise characteristics. A blind deconvolution method assumes the observed image as an auto-regressive moving-average (ARMA) process. In this method, the modeling error of the auto-regressive (AR) process is considered as noise, and the parameters of moving-average (MA) process is considered as an image degradation factor [4-6]. Most blind deconvolution methods, however, cannot guarantee consistent performance with various images and noise characteristics.

A practical approach to estimate the regularization parameters instead of directly obtaining the noise power uses either discrepancy principle [7] or generalized cross-validation [8]. These methods require a high computational load due to the nature of the iterative estimation, and cannot be considered a solution of a practical, real-time image restoration. Another method to estimate the optimal regularization parameter uses the L-curve. Each point on the L-curve in the two-dimensional (2D) coordinate represents the energy of residual error and signal energy calculated using the corresponding regularization parameter. Because this curve generally has the "L" shape, the regularization parameter corresponding to the highest curvature point is considered to be the optimal value [9]. The U-curve method is a variant of the L-curve method [10]. Both L-curve and U-curve methods require a large number of imager restoration processes with various regularization parameters, and are unsuitable for practical applications.

Modeling or analyzing noise has become a fundamental problem in the signal processing area [11]. In speech signal processing, the minimum statistics (MS) method is used widely to estimate ambient noise power under the assumption that there are breaking periods between words in human speech [12]. In other words,a speech-absent period contains only noise components, and its signal power is estimated using a windowed Fourier transform to obtain the noise power.

To apply the MS approach to estimate the noise in an image, it is important to note that there is no signal-absent region in a general image, and that a flat region can play the role of an absent period without a direct current (DC) component. In the flat region, the low-frequency component contains the DC component of the signal, and the high-frequency component contains only noise. In this context the proposed noise power estimation method uses a discrete wavelet transform to decompose the different frequency bands while preserving the locations. Multi-resolution wavelet transform can extract the flat regions, and the noise power is estimated by calculating the signal energy of the corresponding high-frequency component.

This paper is organized as follows. Section 2 explains the image degradation model including the point spread function (PSF) and noise, and briefly presents the basic terminologies for the multiresolution discrete wavelet transform. Section 3 presents the proposed MS-based noise power estimation method for a parametric image restoration. Section 4 summarizes the experimental results of noise power estimation and parametric image restoration, and section 5 concludes the paper.

2. Theoretical Background

2.1 Image Degradation Model

In digital image processing, the general, discrete model for linear degradation caused by blurring and additive noise can be expressed as the following superposition summation,

$$y(i,j)=\sum_{k=1}^{M}\sum_{l=1}^{N}\left(h(i,j;k,1)\cdot f(k,l)\right)+n(i,j), \qquad (1)$$

where $f(i,j)$ represents an original $M\times N$ image, and $h(i,j;k,l)$ is the 2D PSF of the imaging system. The $h(i,j;k,l)$ operator, and $n(i,j)$ additive noise, which is normally modeled as a white Gaussian process. In this paper, it was assumed that the PSF linear space invariant (LSI) is

$$\begin{aligned} y(i,j)&=\sum_{k=1}^{M}\sum_{l=1}^{N}\left(h(i,j;k,1)\cdot f(k,l)\right)+n(i,j)\\ &=h(i,j)**f(i,j)+n(i,j)\end{aligned}, \qquad (2)$$

where ** indicates a 2D convolution. Using the LSI image degradation model in (2), the PSF does not change over the entire image. A major advantage of the LSI model is to reduce the computational load significantly using frequency domain processing.

2.2 Discrete Wavelet Transform

The discrete wavelet transform passes the input signal through a series of filters. A signal can be decomposed into a set of band-limited components, called sub-bands, which can be reassembled to reconstruct the original image without error. As shown in Fig. 1, both sub-bands, which are outputs of $h_0(n)$ and $h_1(n)$, can be downsampled without any loss of information because the bandwidth is smaller than that of the original signal. $h_0(n)$ and $h_1(n)$ are called analysis filters, and $g_0(n)$ and $g_1(n)$ are called synthesis filters. The output of the low-pass filter $h_0(n)$ represents an approximation of $x(n)$, and the output of the high-pass filter $h_1(n)$ represents a detailed part of $x(n)$.

The reconstructed signal $\hat{x}(n)$ is obtained by adding the upsampled and filtered version of $y_0(n)$ and $y_1(n)$. For

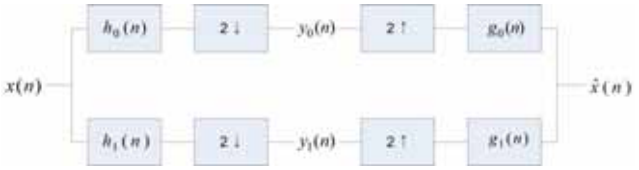

Fig. 1. Two-band filter bank overview.

error-free construction, $\hat{x}(n) = x(n)$, the following conditions must be satisfied.

$$\begin{aligned} H_0(-z)G_0(z) + H_1(-z)G_1(z) &= 0, \\ H_0(z)G_0(z) + H_1(z)G_1(z) &= 2, \end{aligned} \tag{3}$$

where $H_i(z)$ and $G_i(z)$, $i \in \{0,1\}$, respectively represent z-transforms of $h_i(n)$ and $g_i(n)$. (3)is called the conditions for perfect reconstruction.

After some algebraic step, the conditions in (3)are expressed as the following biorthogonality constraint:

$$\langle h_i(2n-k), g_j(k) \rangle = \delta(i-j)\delta(n), \quad i, j \in \{0,1\}, \tag{4}$$

which is imposed on the analysis and synthesis filter impulse responses of all two-band, real-coefficient, perfect reconstruction filter banks.

If the filters are constrained further to be orthonormal, such as

$$\langle g_i(n), g_j(n+2m) \rangle = \delta(i-j)\delta(m), \quad i, j \in \{0,1\}, \tag{5}$$

given a synthesis low-pass filter, g_0, impulse responses h_0, h_1, and g_1 can be determined as follows:

$$\begin{aligned} g_1(n) &= (-1)^n g_0(2K-1-n) \\ h_i(n) &= g_i(2K-1-n) \end{aligned}, \quad i, j \in \{0,1\}, \tag{6}$$

where $2K$ represents the length of each filter.

3. Multiresolution Analysis for a Noise Power Estimation

As stated in section 2, the DWT can effectively search flat areas within an image. On the other hand, the coefficient in each high-pass sub-band contains both signal detail and noise. For the decomposition, they can be classified into the signal detail and pure noise parts. For this, in (2), the input image is expressed as a sum of low-pass and high-pass filtered signals,

$$y(i,j) = h(i,j) ** f_{low}(i,j) + h(i,j) ** f_{high}(i,j) + n(i,j), \tag{7}$$

where f_{high} and f_{low} represent the high-frequency and low-frequency parts, respectively. By applying the DWT,

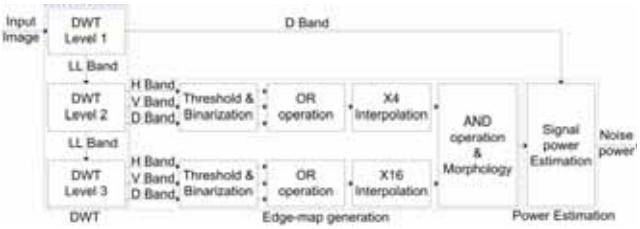

Fig. 2. Block diagram of the proposed algorithm.

(a) (b)

Fig. 3. 3-level DWT (a) the pyramid of DWT sub-bands, (b) corresponding example using Lena image.

(7) can be formulated as

$$\begin{aligned} y_{low}(i,j) &= h(i,j) ** f_{low}(i,j), \quad and \\ y_{high}(i,j) &= h(i,j) ** f_{high}(i,j) + n(i,j). \end{aligned} \tag{8}$$

Because the noise is a random signal, most of $n(i,j)$ is included in the high-frequency sub-band of the DWT. Using the 3-level DWT, the location of the detailed edge $h(i,j) ** f_{high}(i,j)$, is detected, and the noise power can be estimated by excluding the edge region.

Fig. 1 shows a block diagram of the proposed algorithm.

As shown in Fig. 2, the proposed noise power estimation algorithm is composed of three steps, such as 3-level DWT, edge-map generation, and signal power estimation.

3.1 Part of DWT

The proposed algorithm first performs the 3-level DWT, as shown in Fig. 3.

Multiresolution analysis becomes possible by alternative wavelet transforms along each direction. In all subsequent decompositions, the approximation sub-band, which is the sub-image located at the upper-left-hand corner of the previous decomposition, becomes the input for the next level DWT. Each decomposition produces four quarter-size output images that are arranged, as shown in Fig. 3 and substituted for the input from which they were derived. Based on both theoretical and experimental observations, the 2nd and 3rd level DWTs could extract the pure noisy region from the meaningful entities of the original image. In particular, the 1st level diagonal detail component contains both a meaningful edge and noise,

among which only the edge regions are removed using the higher-level detail components.

3.2 Edge-map Generation in the DWT-Space

This subsection describes how the edge map is generated to distinguish the flat regions in an image. In this study, the flat region detection is motivated by the detection of a speech absent period in speech processing. In general, it is difficult to detect the edge using only the signal level DWT when the image contains a substantial amount of noise. Therefore, the 2nd and 3rd level DWT are also needed to extract the edges. The edge-map in the 2nd and 3rd level detail coefficients are defined using the binarization function as follows:

$$e_i[m,n] = \begin{cases} 1, & if\ |x_i[m,n]| > t \\ 0, & otherwise \end{cases}, \text{ for } i \in \{V,H,D\}, \quad (9)$$

where $|x_V|, |x_H|$, and $|x_D|$ respectively represent the absolute values of vertical, horizontal, and diagonal details in the DWT. The threshold values for each level are chosen experimentally as

$$\begin{aligned} t_{2-level} &= (5\times\max + 4\times\min)/9, \\ t_{3-level} &= (5\times\max + 3\times\min)/8, \end{aligned} \quad (10)$$

where max and min represent the biggest and smallest wavelet coefficients, respectively.

After the edge map values e_i are located, they are integratedas follows:

$$e_l(m,n) = e_V(m,n) \cup e_H(m,n) \cup e_D(m,n), \quad \text{for } l = \{2,3\}. \quad (1)$$

The wavelet transform reorganizes the image content into a low-resolution approximation and a set of details of different orientations and different scales. Therefore, the sizes of these edge-maps are smaller than the original image because of the down-sampling by 2 at each level. Therefore, they are used to relocate the edge in the 1st level DWT. The nearest neighbor interpolation was used to register the differently scaled edge maps.

Because the 3rd level DWT coefficients are generated by low-pass filtering signals twice, the corresponding detail components contain only significant edges without random noise. Therefore the resulting edge map can be expressed as

$$e(m,n) = [e_2(m,n)]_2 \cap [e_3(m,n)]_4, \quad (12)$$

where $[e_2(m,n)]_2$ represents the 2nd level edge map upsampled by 2, and $[e_3(m,n)]_4$ is the 3rd level edge map upsampled by 4.

The morphological dilation operation near the edge is used to avoid the case where the details are classified as low components near the sharp edges. The dilation operation is expressed as

$$e_M(m\pm1, n\pm1) = \begin{cases} 1, & if\ e(m,n) = 1 \\ 0, & otherwise \end{cases}. \quad (13)$$

The dilated edge-map provides a better chance to accurately locate the edges in the original image. Therefore, the pixels along the resulting edge are not used, and the other pixels in the flat region serve as a feasible region for a noise power estimation.

3.3 Estimating the noise power

As mentioned in section 2, the noise is defined as a zero mean Gaussian random signal with an autocorrelation as follows:

$$r_{NN}(\tau) = E[N(t)N(t+\tau)] = \sigma^2\delta(\tau), \quad (14)$$

where σ^2 represents the variance, E is the expectation operation, and $\delta(\tau)$ is the unit impulse. The power spectrum of noise is given by the Fourier integration as follows:

$$P_{NN}(f) = \int_{-\infty}^{\infty} r_{NN}(t) e^{-j2\pi ft} dt = \sigma^2. \quad (15)$$

The power spectrum expression in (15) justifies that the variance of a signal-absent region is equal to the constant the noise power spectrum. Given the measured noise variance, the flat region in the 1st level diagonal detail band is taken as follows

$$N(m,n) = \begin{cases} x_D(m,n), & if\ e_M(m,n) = 0 \\ 0, & otherwise \end{cases}, \quad (16)$$

where x_D represents the 1st level diagonal detail band, N is the estimated set of noise samples in the signal-absent region. Finally the noise power is computed as follows:

$$\begin{aligned} \sigma^2 &= \frac{1}{TN}\sum_{m=1}^{I}\sum_{n=1}^{J}\left(N(m,n) - E\left(N(m,n)\right)\right)^2, \\ TN &= I\times J - (\text{Total number of } e_M = 1), \end{aligned} \quad (17)$$

where I and J respectively represent the vertical and the horizontal sizes of the diagonal detailband in the 1st level DWT, and TN is the number of samples in the flat region.

4. Experimental Results

This section presents the simulation results of the proposed noise power estimation algorithm and its application to parametric image restoration algorithms. A set of standard 256×256 8-bit grayscale images were tested including Lena, Cameraman, Barbara, Boat, and Goldhill. These test images were degraded by simulating 3

Table 1. Results of noise estimation (variance of noise).

Image	Blur Size	SNR [dB]							
		0	10	20	30	40	50	60	70
Lena	Real Value	3239.667	323.9667	32.3967	3.2397	0.324	0.0324	0.0032	0.0003
	3x3	3210.103	328.7249	33.5885	4.4679	1.5785	1.2934	1.2687	1.2671
	5x5	3221.812	330.5618	32.8476	3.4774	0.5635	0.2797	0.2532	0.25
	7x7	3209.968	328.8707	32.4743	3.3669	0.4416	0.1513	0.1229	0.1203
	9x9	3226.263	326.8065	32.7087	3.2984	0.3854	0.0964	0.0685	0.066
	11x11	3254.237	324.4781	32.698	3.2888	0.3587	0.0671	0.0386	0.036
Camera-man	Real Value	4210.47	421.047	42.1047	4.2105	0.421	0.0421	0.0042	0.0004
	3x3	4289.119	427.3593	44.7465	6.6499	2.8844	2.4891	2.4563	2.4542
	5x5	4275.86	425.0564	43.0084	4.7718	0.9294	0.5445	0.5052	0.501
	7x7	4285.852	424.2836	42.5722	4.4455	0.6188	0.2322	0.1939	0.1895
	9x9	4263.994	425.6784	42.3067	4.3027	0.5046	0.1252	0.0872	0.0836
	11x11	4249.764	424.5425	42.2741	4.2588	0.4648	0.0845	0.0464	0.042
Barbara	Real Value	2792.166	279.2166	27.9217	2.7922	0.2792	0.0279	0.0028	0.0003
	3x3	2898.218	286.6985	33.5393	7.9205	5.5188	5.0846	5.046	5.0325
	5x5	2822.948	286.0339	29.2028	3.661	1.0558	0.7771	0.7441	0.7401
	7x7	2816.222	286.8649	28.8068	3.113	0.5272	0.2626	0.2335	0.23
	9x9	2846.788	287.5493	28.9163	2.9441	0.3874	0.1252	0.0977	0.0946
	11x11	2821.618	287.5812	28.3155	2.9071	0.3304	0.0729	0.0467	0.044
Boat	Real Value	2707.32	270.732	27.0732	2.7073	0.2707	0.0271	0.0027	0.0003
	3x3	2751.544	277.1431	29.4363	4.6828	2.2253	1.984	1.962	1.9604
	5x5	2771.077	276.8141	28.0699	3.1505	0.6464	0.3948	0.3692	0.3664
	7x7	2758.934	276.0354	27.7257	2.8803	0.3901	0.1426	0.1189	0.1165
	9x9	2728.934	274.6365	27.607	2.8073	0.3229	0.0739	0.0489	0.0464
	11x11	2742.365	274.4742	27.4036	2.7858	0.2992	0.0495	0.0246	0.0222
Goldhill	Real Value	2133.844	213.3844	21.3384	2.1338	0.2134	0.0213	0.0021	0.0002
	3x3	2173.891	217.3611	22.407	2.9837	1.0581	0.8544	0.8344	0.8321
	5x5	2137.604	216.0309	21.7738	2.3268	0.3832	0.1885	0.168	0.1658
	7x7	2106.107	215.7399	21.8678	2.2283	0.2727	0.0776	0.0573	0.0554
	9x9	2140.056	216.8333	21.5465	2.1786	0.2404	0.046	0.0267	0.0248
	11x11	2171.393	214.9948	21.1543	2.1046	0.2216	0.0349	0.0164	0.0147

to 11 pixel uniform blurs with additive Gaussian white noise of 0 to 70dB SNR. The proposed method was then used to estimate the noise power for each image to evaluate the performance of the estimation method. Table 1 shows the experimental results by comparing the real and estimated noise powers.

The numerical data given in Table 1 are the real and estimated values. As shown in Table 1, the proposed estimation method gives accurate noise power values with SNR 0 to 30dB, which is illustrated in Fig. 4 for the Lena image.The vertical axis of the graph in Fig. 4 represents the level noise power on a log scale, and the horizontal axis indicates the SNR values. For images with SNR 0 to 30dB, the estimated noise powers were similar to the real noise power regardless of the blur sizes. As the SNR was increased above 40dB, the number of noise samples decreased. On the other hand, for images with SNR 40dB or higher, the number of detected noise samples decreased significantly and the estimation accuracy decreased. Larger blur sizes provide a more accurate estimation with SNR 40dB or higher because it suppresses more edge in the original image.

Table 2 shows the image restoration results of the Wiener filter using estimated noise power. Given the

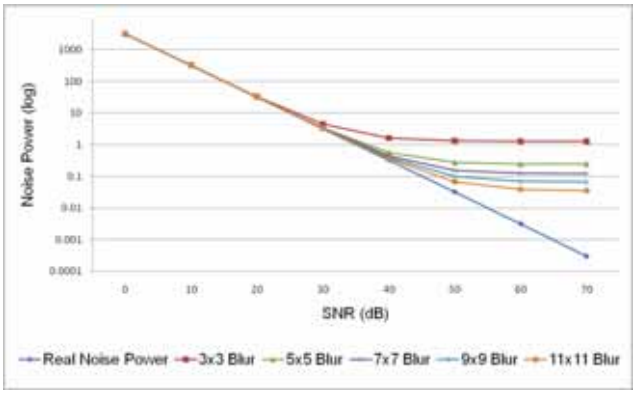

Fig. 4. Result of noise estimation fromthe Lena image.

spectrum of the original image, the Wiener filter can theoretically minimize the mean squared error between the original and restored images with the frequency responses as follows:

$$W(u,v) = \frac{H^*(u,v)}{\left|H(u,v)\right|^2 + S_{\eta\eta}(u,v)/S_{xx}(u,v)}, \quad (18)$$

Table 2. Results of image restoration using the Wiener filter with the real and the estimated noise power (peak-to-peak signal-to-noise ratio; PSNR).

Image	Blur Size	Type of noise power	SNR [dB]							
			0	10	20	30	40	50	60	70
Lena	3x3	Real	23.8846	26.9816	29.8579	32.6848	35.8671	39.4885	43.4946	47.7143
		Estimated	23.4047	26.5427	29.3919	32.1093	34.2927	34.9086	34.9831	34.9906
	5x5	Real	23.0575	25.2821	27.3222	29.4897	32.0639	35.221	39.0044	43.1626
		Estimated	22.675	24.9369	26.9202	29.0259	31.4048	32.9659	33.2785	33.311
	7x7	Real	22.3753	24.1837	25.8135	27.6967	30.06	33.0215	36.5146	40.5006
		Estimated	22.065	23.856	25.4184	27.2461	29.5475	31.5776	32.173	32.2479
	9x9	Real	21.759	23.3895	24.899	26.6741	28.8624	31.4747	34.6416	38.339
		Estimated	21.4581	23.0627	24.4949	26.2692	28.3943	30.5291	31.3855	31.5106
	11x11	Real	21.1039	22.6819	24.2392	25.9698	28.0801	30.6281	33.7327	37.367
		Estimated	20.868	22.3391	23.864	25.5693	27.6278	29.8919	31.114	31.3166
Cameraman	3x3	Real	22.3852	25.1677	27.9766	30.9808	34.2485	37.7331	41.5757	45.8096
		Estimated	21.9164	24.6894	27.4516	30.3447	32.3317	32.8001	32.8573	32.8652
	5x5	Real	21.5558	23.5775	25.5864	27.9729	30.7363	33.8736	37.467	41.2927
		Estimated	21.2098	23.1896	25.1141	27.4553	29.9248	31.1618	31.3714	31.3946
	7x7	Real	20.9223	22.5638	24.3757	26.5466	29.0746	31.9082	35.2263	39.1707
		Estimated	20.6341	22.2235	23.9819	26.0993	28.4755	30.3097	30.7895	30.851
	9x9	Real	20.449	21.8927	23.4982	25.4301	27.6668	30.2777	33.4247	37.0752
		Estimated	20.1916	21.5898	23.1314	24.9955	27.163	29.2284	30.065	30.1846
	11x11	Real	20.0748	21.4623	22.9824	24.7365	26.7858	29.2677	32.2804	35.957
		Estimated	19.8498	21.154	22.648	24.3485	26.3084	28.5152	29.794	30.0443
Barbara	3x3	Real	22.1229	23.7675	25.514	27.8749	30.9784	34.6997	38.7562	43.0572
		Estimated	21.8203	23.4125	25.0313	26.9306	27.7802	27.9562	27.9747	27.9797
	5x5	Real	21.628	22.8247	23.8684	25.397	27.8021	31.0406	34.8908	39.3204
		Estimated	21.4152	22.6156	23.5383	24.8888	26.5741	27.2407	27.34	27.3524
	7x7	Real	21.2283	22.2636	23.1719	24.3456	26.097	28.8169	32.1934	35.9993
		Estimated	21.0226	22.0707	22.9196	23.9757	25.446	26.5676	26.8225	26.8576
	9x9	Real	20.8446	21.8374	22.7304	23.8295	25.4918	27.9728	31.213	34.937
		Estimated	20.6408	21.6444	22.506	23.4944	24.9746	26.5974	27.1552	27.2373
	11x11	Real	20.5045	21.5016	22.3495	23.2996	24.6436	26.761	29.7923	33.4748
		Estimated	20.2965	21.2833	22.1469	23.0199	24.1927	25.8614	26.7647	26.9174
Boat	3x3	Real	24.0632	27.1509	30.2964	33.6468	37.273	41.2964	45.6637	50.1293
		Estimated	23.5584	26.6655	29.8074	32.9608	35.0155	35.4524	35.5005	35.504
	5x5	Real	23.1033	25.2132	27.4282	30.0571	33.1536	36.719	40.7213	44.9659
		Estimated	22.7406	24.7927	26.9735	29.5745	32.2789	33.6228	33.8489	33.8718
	7x7	Real	22.4804	24.1381	26.1268	28.5302	31.3814	34.6481	38.3193	42.4117
		Estimated	22.1738	23.7767	25.6666	28.0361	30.8162	33.0273	33.6076	33.6758
	9x9	Real	22.0587	23.6051	25.3004	27.3715	29.9533	32.897	36.2837	40.2263
		Estimated	21.782	23.2519	24.8722	26.8895	29.459	31.951	33.018	33.1789
	11x11	Real	21.5606	22.9538	24.623	26.6416	29.0169	31.766	34.9755	38.7398
		Estimated	21.3145	22.6123	24.2556	26.1988	28.4963	31.0803	32.7101	33.0407
Goldhill	3x3	Real	26.7398	30.2543	33.746	37.3324	41.0328	44.8544	48.9565	53.1223
		Estimated	26.255	29.7393	33.2195	36.7474	39.407	40.1518	40.2293	40.2368
	5x5	Real	25.8456	28.4774	31.0497	33.9961	37.2998	40.8006	44.5499	48.6226
		Estimated	25.4779	28.035	30.5548	33.4822	36.5811	38.4764	38.8736	38.9279
	7x7	Real	25.1182	27.3499	29.6478	32.1777	35.0686	38.1718	41.6039	45.5468
		Estimated	24.766	26.961	29.179	31.7038	34.5376	37.0044	37.8739	37.9951
	9x9	Real	24.4436	26.45	28.5452	31.056	33.8238	36.7732	40.1019	43.819
		Estimated	24.0947	26.0663	28.1484	30.5624	33.2791	35.9845	37.3805	37.6098
	11x11	Real	23.8268	25.5836	27.5896	29.9754	32.5945	35.4005	38.5675	42.2403
		Estimated	23.5211	25.2339	27.1688	29.4912	32.0828	34.8182	36.5704	36.9412

where S_{xx} and $S_{\eta\eta}$ represent the power spectra of the original image and noise, respectively.

In most image restoration problems, the power spectrum information of the original image is unavailable. The original Wiener filter, however, provides the good reference for comparing a range of image restoration algorithms. For the experiment the original periodogram was used as an approximation of S_{xx}. The MSE for PSNR of the restored image was calculated as

$$MSE = \frac{1}{m \times n} \sum_{i=0}^{m-1} \sum_{j=0}^{n-1} \left\| f(i,j) - \hat{f}(i,j) \right\|^2, \qquad (19)$$

Table 3. Results of image restoration using the parametric Wiener filter with $K_{est} = \left(\alpha\sigma_{\eta}^{2}\right)^{1/\gamma}$.

Image	Blur Size	Type of NSPR	SNR [dB]							
			0	10	20	30	40	50	60	70
Lena	3x3	K	15.9318	21.1556	26.3624	30.8127	34.4406	38.1502	42.2265	46.6949
		Estimated	15.5051	20.0607	24.8053	29.8786	34.261	35.7159	35.9104	35.9207
	5x5	K	17.4361	21.7755	25.3427	28.0514	30.5762	33.5892	37.2297	41.5856
		Estimated	17.1252	21.1244	24.4503	27.5974	30.3498	31.7327	31.9689	31.9935
	7x7	K	18.2425	21.796	24.3586	26.35	28.4543	30.7008	34.8828	39.0884
		Estimated	17.7177	21.4231	23.9424	26.1339	28.0718	29.2616	29.5343	29.5684
	9x9	K	18.6639	21.6007	23.6512	25.4092	27.3613	29.8073	32.9877	36.867
		Estimated	17.8185	21.2934	23.4131	25.172	26.7803	27.9153	28.2355	28.2727
	11x11	K	18.8018	21.2345	22.9586	24.6046	26.5019	28.887	31.9835	35.8382
		Estimated	17.6566	20.8506	22.6883	24.2065	25.6444	26.8167	27.2505	27.3095
Cameraman	3x3	K	14.83	20.0254	24.9753	29.1312	32.7159	36.3606	40.3133	44.7693
		Estimated	14.5677	19.3279	24.0353	28.7647	32.1538	33.031	33.1424	33.1552
	5x5	K	16.2889	20.4608	23.7696	26.4517	29.1533	32.2267	35.7827	39.984
		Estimated	15.9452	20.0983	23.324	26.258	28.6586	29.6334	29.7835	29.8008
	7x7	K	17.0884	20.5188	23.0076	25.1551	27.4511	30.2898	33.7674	37.763
		Estimated	16.3905	20.2704	22.7929	24.9561	26.8537	27.9151	28.133	28.1587
	9x9	K	17.4939	20.3244	22.2864	24.1143	26.148	28.6795	31.841	35.7081
		Estimated	16.4573	20.0455	22.1054	23.815	25.3987	26.4971	26.8065	26.8474
	11x11	K	17.7483	20.1703	21.864	23.5494	25.3692	27.7015	30.7469	34.5304
		Estimated	16.417	19.8031	21.6284	23.1215	24.5419	25.6682	26.0991	26.1714
Barbara	3x3	K	15.6221	20.2254	23.8989	26.6357	29.857	33.7201	37.7904	42.2838
		Estimated	15.1585	19.3323	23.2726	26.3977	27.5048	27.6864	27.7061	27.7081
	5x5	K	17.0036	20.596	22.9081	24.4345	26.6259	29.8918	33.7617	38.1397
		Estimated	16.6052	20.0261	22.4073	24.2798	25.473	25.8018	25.846	25.8513
	7x7	K	17.7924	20.7061	22.4257	23.616	25.1575	27.701	31.1878	34.9679
		Estimated	17.2068	20.3588	22.1394	23.4625	24.4797	24.93	25.0101	25.023
	9x9	K	18.25	20.6639	22.0591	23.1151	24.5087	26.9901	30.3902	34.1428
		Estimated	17.3746	20.3733	21.8667	22.932	23.8154	24.361	24.4941	24.5111
	11x11	K	18.4585	20.5093	21.7195	22.6843	23.7905	25.7951	28.9341	32.7194
		Estimated	17.3491	20.1864	21.5347	22.4634	23.2328	23.7866	23.9701	23.9954
Boat	3x3	K	15.4863	20.9674	26.437	31.2731	35.182	39.3307	43.6906	48.6787
		Estimated	15.1861	20.1418	25.1831	30.609	34.9407	36.149	36.2982	36.3096
	5x5	K	17.0373	21.5494	25.3366	28.3519	31.2236	34.2817	38.1526	42.7778
		Estimated	16.6487	21.0308	24.6194	27.9757	30.7804	31.9434	32.124	32.1461
	7x7	K	17.9772	21.7346	24.5518	26.8864	29.2883	32.326	36.1975	40.5773
		Estimated	17.2375	21.3906	24.2071	26.6575	28.8158	30.0834	30.3524	30.381
	9x9	K	18.545	21.7533	24.0697	26.0827	28.2278	30.8949	34.2007	38.2447
		Estimated	17.4206	21.3988	23.8148	25.8097	27.6224	28.9701	29.4022	29.4615
	11x11	K	18.8042	21.496	23.4107	25.2646	27.3417	29.8694	33.028	36.8845
		Estimated	17.3771	21.0831	23.1355	24.832	26.4608	27.8568	28.4567	28.5564
Goldhill	3x3	K	17.292	22.7483	28.4208	33.684	38.0951	42.0161	46.0533	50.8886
		Estimated	16.6058	21.1164	26.1581	31.871	37.8767	40.7316	41.1952	41.2456
	5x5	K	18.9349	23.6931	27.9453	31.4699	34.6221	37.9221	41.6176	46.2508
		Estimated	18.5681	22.5305	26.3129	30.295	34.341	36.966	37.5577	37.6266
	7x7	K	19.921	24.0243	27.3415	30.13	32.7592	35.5151	39.0593	43.1829
		Estimated	19.5879	23.3945	26.527	29.6315	32.547	34.6976	35.3421	35.4257
	9x9	K	20.4684	23.9485	26.6062	29.0018	31.4507	34.2092	37.4553	41.3001
		Estimated	19.9582	23.5935	26.2212	28.7512	31.1578	33.1109	33.8879	33.9952
	11x11	K	20.7242	23.6782	25.8681	27.9547	30.2072	32.8143	36.0581	39.7016
		Estimated	19.9897	23.3871	25.6156	27.69	29.717	31.4794	32.3138	32.4576

where m and n respectively represent the vertical and the horizontal sizes of image, and f and $\hat{f}$ respectively represent the original and the restored images.

Finally, The PSNR of the restored image was computed as

$$PSNR = 10 \times \log_{10}\left(\frac{255^2}{MSE}\right). \quad (20)$$

Fig. 5 shows the PSNR values of the restored Lena image by the Wiener filter using both real and the estimated noise power.

Table 4. Results of image restoration using the ForWaRD algorithm in PSNR.

Image	Blur Size	Type of noise power	SNR [dB]							
			0	10	20	30	40	50	60	70
Lena	3x3	Real	12.0817	23.6813	29.2859	31.9092	34.4559	36.8064	39.6032	43.3297
		Estimated	12.0868	23.6758	29.3248	32.1796	34.144	34.6094	34.6619	34.668
	5x5	Real	11.7382	22.4076	26.9339	29.2023	31.5026	33.9945	36.6331	39.3912
		Estimated	11.8118	22.3772	26.9357	29.2575	31.5324	32.6363	32.8197	32.8464
	7x7	Real	11.4096	21.3742	25.424	27.5061	29.7853	32.403	35.0823	37.8321
		Estimated	11.3242	21.3668	25.4212	27.5169	29.7972	31.4571	31.8569	31.9074
	9x9	Real	11.1004	20.4556	24.3463	26.4596	28.6033	31.0552	33.6474	36.4111
		Estimated	11.1417	20.4478	24.3411	26.4575	28.616	30.551	31.2091	31.3036
	11x11	Real	10.8212	19.6835	23.4171	25.5444	27.7366	30.2433	32.9371	35.797
		Estimated	10.8649	19.6606	23.4118	25.5407	27.7343	30.0629	31.2289	31.4529
Cameraman	3x3	Real	11.0517	22.4179	27.873	30.6476	33.3845	36.1039	39.1418	42.8819
		Estimated	10.9414	22.3433	27.8843	30.6871	32.2059	32.5164	32.554	32.556
	5x5	Real	10.7765	21.0941	25.4287	28.0118	30.4362	32.9708	35.8083	38.8658
		Estimated	10.6758	21.0289	25.419	28.0188	30.3005	31.3138	31.4702	31.4753
	7x7	Real	10.561	20.291	24.1672	26.5228	28.9035	31.4477	34.1255	37.1174
		Estimated	10.4758	20.2319	24.1577	26.524	28.8491	30.433	30.8025	30.8504
	9x9	Real	10.3691	19.5755	23.0402	25.3061	27.5775	30.0886	32.8474	35.723
		Estimated	10.3303	19.5142	23.0302	25.2988	27.5672	29.5916	30.3182	30.4176
	11x11	Real	10.2108	19.0828	22.4008	24.5842	26.7784	29.2419	31.9406	34.9117
		Estimated	10.2051	19.0236	22.3881	24.5751	26.7639	29.0231	30.1878	30.3834
Barbara	3x3	Real	11.0449	21.2378	24.7526	26.9164	30.1828	33.8312	37.5026	41.9574
		Estimated	10.8148	21.087	24.6716	26.0643	26.5323	26.6119	26.6176	26.6209
	5x5	Real	10.7637	20.5683	23.4534	24.5723	26.8274	30.3315	34.0291	37.8115
		Estimated	10.5676	20.4787	23.4474	24.4801	25.4027	25.7003	25.735	25.7418
	7x7	Real	10.4977	19.9653	22.8228	23.8457	25.2706	27.9346	31.623	35.3334
		Estimated	10.3799	19.8755	22.8167	23.827	24.9221	25.5157	25.6219	25.6313
	9x9	Real	10.2513	19.4173	22.3375	23.3361	24.6415	27.048	30.586	34.2884
		Estimated	10.1233	19.3608	22.3348	23.3324	24.4798	25.4812	25.758	25.7993
	11x11	Real	10.0229	18.9017	21.8941	22.9549	23.9286	25.8029	29.1708	32.9918
		Estimated	9.9002	18.8099	21.8931	22.954	23.8844	24.8263	25.1891	25.2358
Boat	3x3	Real	10.3301	22.6785	29.4999	32.4216	35.2734	37.9196	41.0248	44.868
		Estimated	10.0789	22.5	29.5178	32.6431	34.7408	35.1895	35.2668	35.2639
	5x5	Real	10.0144	21.4427	26.8712	29.4584	32.0061	34.7688	37.731	40.7402
		Estimated	9.7854	21.227	26.8496	29.4914	32.0153	33.3866	33.6243	33.6423
	7x7	Real	9.7684	20.6427	25.465	27.9147	30.4422	33.1262	35.8268	38.9086
		Estimated	9.6516	20.5446	25.4509	27.9136	30.4533	32.4932	33.0274	33.0795
	9x9	Real	9.553	20.0144	24.6253	26.9061	29.1889	31.7675	34.4731	37.347
		Estimated	9.5524	20.0018	24.6092	26.9015	29.2019	31.5362	32.5181	32.662
	11x11	Real	9.3585	19.4501	23.7401	26.0097	28.2808	30.8416	33.5767	36.5561
		Estimated	9.2723	19.3932	23.7187	25.9944	28.2818	30.7293	32.0985	32.3484
Goldhill	3x3	Real	13.1989	25.4969	32.3482	35.2669	37.8552	40.285	43.2054	46.8622
		Estimated	13.2117	25.3896	32.3882	35.6726	38.1347	38.8696	38.9647	38.9783
	5x5	Real	12.9351	24.466	30.034	32.7458	35.0247	37.3128	39.9765	42.7068
		Estimated	12.8569	24.4952	30.0358	32.8443	35.4271	36.8648	37.1323	37.1505
	7x7	Real	12.6919	23.5989	28.7017	31.1889	33.3095	35.7235	38.2176	40.9962
		Estimated	12.6546	23.6454	28.7035	31.2045	33.5262	35.3785	35.8772	35.9481
	9x9	Real	12.4738	22.8065	27.493	30.0713	32.2931	34.6044	36.9353	39.5736
		Estimated	12.4534	22.8189	27.4957	30.0712	32.3863	34.669	35.5987	35.7388
	11x11	Real	12.2787	22.1495	26.4667	29.0588	31.3209	33.6124	35.9986	38.7593
		Estimated	12.2625	22.1802	26.4651	29.0606	31.357	33.8235	35.3351	35.623

Similar experiments were performed using a parametric Wiener filter with a constant noise-to-signal power ratio (NSPR) as follows:

$$\frac{S_{\eta\eta}}{S_{xx}} \cong K_{est} = \left(\alpha\sigma_{\eta}^{2}\right)^{1/\gamma}, \qquad (21)$$

where experimentally chosen parameters $\alpha = 0.000015446$ and $\gamma = 2$ were used. The near optimal value of K_{est} was obtained by an interactive simulation for the optimal PSNR, where K_{est} is in the range $[1.0\times10^{-8}, 1.0]$. The corresponding PSNR values are given in Table 3. Other experimental results using the manually selected constant for the NSPR are given in Table 4.

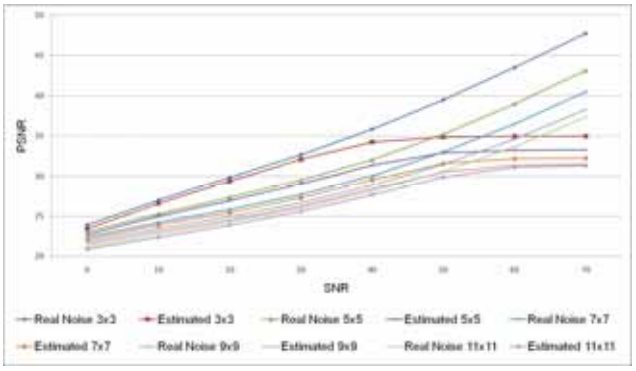

Fig. 5. PSNR values of the Wiener filter versus various noise levels.

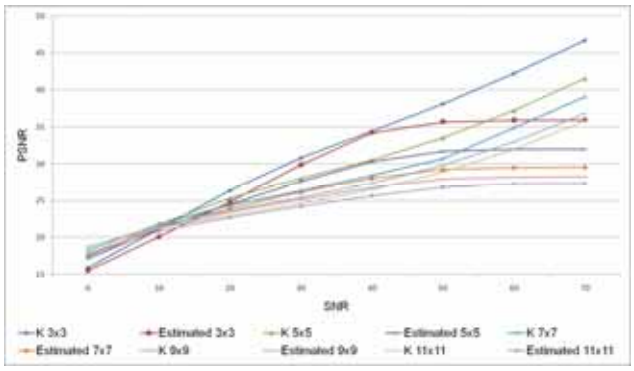

Fig. 6. PSNR values of the restored results using the parametric Wiener filter for the Lena image versus various levels of noise.

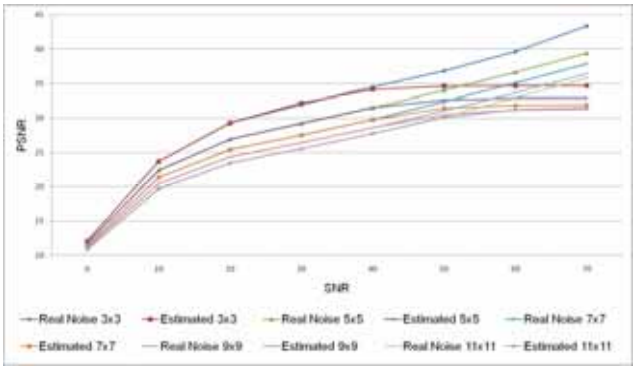

Fig. 7. PSNR values of the restored results using the ForWaRD algorithm for Lena image versus various levels of noise.

In addition to the original and the parametric Wiener filter, this study tested Fourier-Wavelet Regularized Deconvolution (ForWaRD) algorithm, which effectively combines and balances scalar Fourier shrinkage and wavelet shrinkage [13]. Table 5 summarizes the restored results using the ForWaRD algorithm by comparing the PSNRs with the real and estimated noise power. The ForWaRD algorithm was tested on two conditions, one with real noise power and the other with an estimated

Fig. 8. Comparison of the restored images (a) original image, (b) observed image degraded by two dimensional 7×7 uniform blur with 20dB whith Gaussian noise, (c) restored image using the original Wiener filter with real noise power, (d) restored image using the original Wiener filter with the estimated noise power, (e) restored image using the parametric Wiener filter with manually chosen constant NSPR shown in Table 4, (f) restored image using the parametric Wiener filter with the estimated noise power, (g) restored image using the ForWaRD algorithm with real noise power, (h) restored image using the ForWaRD algorithm with the estimated noise power.

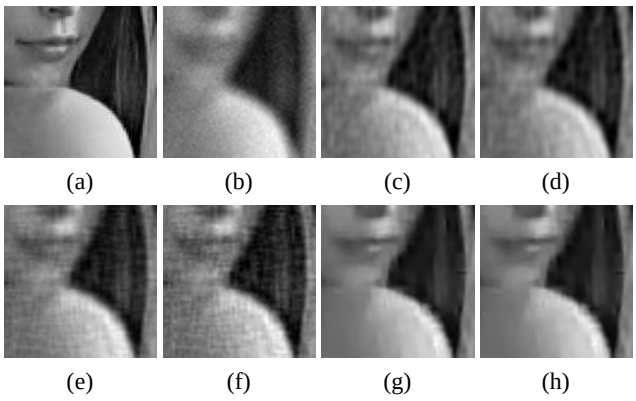

Fig. 9. Magnified images of Fig. 8.

noise power, as shown in Table 5. For images with high level noise, such as SNR 0 to 40dB, the ForWaRD algorithm gives similar restoration performance using both the real and estimated noise power.

Fig. 7 shows the restoration results using the ForWaRD algorithm with real and estimated noise power for the Lena image.

Fig. 8 shows the restored Lena images for the 7×7 uniform blur and 20dB additive noise.

From Fig. 8(c)-(f) exhibit some artifacts due to incomplete reconstruction of the entire frequency components, while the ForWaRD algorithm can reduce such artifacts, as shown in Fig. 8(g) and (h). In addition, there are no differences between the results using the original and estimated noise power.

5. Conclusion

This paper proposed a novel noise power estimation algorithm based on the DWT-based minimum statistics. The estimated noise can be used for any parametric image restoration filter. Based on experimental results, the accuracy of the proposed estimation method was more than 90% with a relatively high noise level of SNR. As the SNR was increased to more than 50dB, the estimation accuracy decreased because the total number of noise samples approaches zero. Such inaccuracy, however, is not a serious problem because the final restored results maintain sufficiently high quality. The proposed algorithm can estimate the noise power far more efficiently than any existing algorithm. In addition, there were almost no differences between the restored results using real and estimated noise power. Because the proposed algorithm estimated noise power in the DWT domain, it can fully utilize multiple resolution characteristics of the noise distribution, and as a result, its estimation results can be applied successfully to any kind of parametric image restoration filters.

Acknowledgement

This studywas supported in part by the Basic Science Research Program through National Research Foundation (NRF) of Korea funded by the Ministry of Education, Science and Technology (2009-0081059, 2013R1A1A2061847).

References

[1] M. Banhamand A. Katsaggelos, “Digital image restoration,”*IEEE Signal Processing Magazine*, vol. 14, no. 2, pp. 24-41, Mar. 1997. Article (CrossRef Link)

[2] S. Chang, Y. Bin, and M. Vetterli,“Adaptive wavelet thresholding for image denoising and compression,” *IEEE Trans. Image Processing*, vol. 9, no. 9, pp.1532-1546, Sep. 2000. Article (CrossRef Link)

[3] L.Ce, R. Szeliski, K. Sing, C. Zitnick, and W. Freeman, “Automatic estimation and removal of noise from a single image,” *IEEE Trans. Pattern Analysis, Machine Intelligence*, vol. 30, no. 2, pp. 299-314, Feb. 2008. Article (CrossRef Link)

[4] A. Tekalp, H. Kaufman, and J. Woods, “Identification of image and blur parameters for the restoration of noncausal blurs,”*IEEE Trans. Acoustics, Speech, Signal Processing*, vol. 34, no. 4, pp. 963-972, Aug. 1986. Article (CrossRef Link)

[5] R. Legendijk, A.Tekalp, and J. Biemond, “Maximum likelihood image and blur identification: a unifying approach,”*Optical Engineering*, vol. 29, no. 5, pp 422-435, May 1990. Article (CrossRef Link)

[6] A. Tekalp and H. Kaufman, “On statistical identification of a class of linear space-invariant blurs using nonminimum-phase arma models,” *IEEE Trans. Acoustics, Speech, Signal Processing*,vol. 38, no. 8, pp. 1360-1363, Aug. 1988. Article (CrossRef Link)

[7] H. Engl, “Discrepancy principles for Tikhonov regularization of ill-posed problems leading to optimal convergence rates,” *Journal of Optimization Theory and Applications*, vol. 52, no. 2, pp. 209-215, 1987. Article (CrossRef Link)

[8] N. Wayrich, and G. Warhola, “Wavelet shrinkage and generalized cross validation for image denoising,” *IEEE Trans. Image Processing*, vol. 7, no.1, pp. 82-90, Jan. 1998. Article (CrossRef Link)

[9] P. Hansen, “Analysis of discrete ill-posed problems by means of the L-curve,”*SIAM Review*, vol. 34, no. 4, pp. 561-580, 1992. Article (CrossRef Link)

[10] D. Krawczyk-Stando, and M. Rudnicki, “Regularization parameter selection in discrete ill-posed problems: the use of the U-curve,” *International Journal of Applied Mathematic Computer Science*, vol. 17, no. 2, pp. 157-164,2007. Article (CrossRef Link)

[11] S. Kayand S. Marple, “Spectrum analysis-A modern perspective,”*IEEE Proceeding*, vol. 69, no. 11, pp. 1380-1419,Nov. 1981. Article (CrossRef Link)

[12] R.Martin, “Noise power spectral density estimation based on optimal smoothing and minimum statistics,” *IEEE Trans. Speech and Audio Processing*, vol. 9, no. 5, pp. 504-512,July 2001. Article (CrossRef Link)

[13] R.Neelamani,H. Choi, and R.Baraniuk,“ForWaRD: Fourier-wavelet regularized deconvolution for ill-conditioned systems,”*IEEE Trans. Signal Processing*, vol. 52, no. 2, pp. 418-433, Feb. 2004. Article (CrossRef Link)

Yoonjong Yoo was born in Seoul, Korea in 1981. He received hisB.S. degree in electronic engineering from Chung-Ang University, Seoul, Korea, in 2005. He received hisM.S. degree in image engineering from Chung-Ang University, Seoul, Korea, in 2007. From 2009 to 2013, he joined Nextchip, where he designed the auto exposure, auto white balance, and wide dynamic range for surveillance camera. Currently, he is pursuing a Ph.D. degree in image processing at Chung-Ang University. His research interests include image enhancement and restoration for display processing, video compression standards and surveillance video applications.

Jeongho Shin received hisB.S. and the M.S. degrees in electronic engineering from Chung-Ang University, Seoul, Korea, in 1994 and 1998, respectively, and Ph.D. degree in image engineering from Chung-Ang University, Seoul, Korea, in 2001. From 2003 to 2006, he was a research professor at the department of image engineering, Chung-Ang University, Seoul, Korea. Currently, he is an assistant professor at the department of web information engineering, Hankyong National University, Gyeonggi, Korea. His current research interests include the enhancement and restoration of image and video, object tracking, and data fusion.

Joonki Paik was born in Seoul, Korea in 1960.He received hisB.S. degree in control and instrumentation engineering from Seoul National University in 1984.He received hisM.S. and the Ph.D. degrees in electrical engineering and computer science from North-western University in 1987 and 1990, respectively. From 1990 to 1993, he joined Samsung Electronics, where he designed the image stabilization chip sets for consumer's camcorders.Since 1993, he has joined the faculty at Chung-Ang University, Seoul, Korea, where he is currently a Professor in the Graduate school of Advanced Imaging Science, Multimedia and Film. From 1999 to 2002, he was a visiting Professor at the Department of Electrical and Computer Engineering at the University of Tennessee, Knoxville. Dr. Paik was a recipient of the Chester-Sall Award from the IEEE Consumer Electronics Society, Academic Award from the Institute of Electronic Engineers of Korea, and Best Research Professor Award from Chung-Ang University. He has served the Consumer Electronics Society of IEEE as a member of the Editorial Board. Since 2005, he has been the head of National Research Laboratory in the field of image processing and intelligent systems. In 2008, he has worked as a full-time technical consultant for the System LSI Division in Samsung Electronics, where he developed various computational photographic techniques including an extended depth of field (EDoF) system. From 2005 to 2007 he served as Dean of the Graduate School of Advanced Imaging Science, Multimedia, and Film. From 2005 to 2007 he has been Director of Seoul Future Contents Convergence (SFCC) Cluster established by Seoul Research and Business Development (R&BD) Program. Dr. Paik is currently serving as a member of the Presidential Advisory Board for Scientific/Technical policy of Korean Government and a technical consultant of Korean Supreme Prosecutor's Office for computational forensics.